Available online at www.sciencedirect.com
ScienceDirect
Geochimica et Cosmochimica Acta 75 (2011) 4140–4156
Geochimica et Cosmochimica Acta
www.elsevier.com/locate/gca

Oxygen and carbon isotopic systematics of aragonite speleothems and water in Furong Cave, Chongqing, China

Ting-Yong Li [a,b,c,d], Chuan-Chou Shen [d,*], Hong-Chun Li [d,e], Jun-Yun Li [a], Hong-Wei Chiang [d], Sheng-Rong Song [d], Dao-Xian Yuan [a,f], Chris D.-J. Lin [d], Pan Gao [g], Liping Zhou [g], Jian-Li Wang [a,c], Ming-Yang Ye [a], Liang-Liang Tang [h], Shi-You Xie [a,c]

[a] *School of Geographical Sciences, Southwest University, Chongqing 400715, China*
[b] *State Key Laboratory of Loess and Quaternary Geology, Institute of Earth Environment, CAS, Xi'an 710075, China*
[c] *Key Laboratory of the Three Gorges Reservoir Region's Eco-Environment, Chongqing University and Southwest University, Ministry of Education, Chongqing 400715, China*
[d] *High-Precision Mass Spectrometry and Environment Change Laboratory (HISPEC), Department of Geosciences, National Taiwan University, Taipei 10617, Taiwan, ROC*
[e] *Department of Earth Sciences, National Cheng-Kung University, Tainan 70101, Taiwan, ROC*
[f] *Karst Dynamics Laboratory, Institute of Karst Geology, CAGS, Guilin 541004, China*
[g] *Department of Geography, Peking University, Beijing 100871, China*
[h] *Administration of Scenic and Historic Interest, Wulong County, Chongqing 408500, China*

Received 11 November 2010; accepted in revised form 6 April 2011; available online 14 April 2011

Abstract

To understand oxygen and carbon stable isotopic characteristics of aragonite stalagmites and evaluate their applicability to paleoclimate, the isotopic compositions of active and fossil aragonite speleothems and water samples from an *in situ* multi-year (October 2005–July 2010) monitoring program in Furong Cave located in Chongqing of China have been examined. The observations during October 2005–June 2007 show that the meteoric water is well mixed in the overlying 300–500-m bedrock aquifer, reflected by relatively constant $\delta^{18}O$, ±0.11–0.14‰ (1σ), of drip waters in the cave, which represents the annual status of rainfall water. Active cave aragonite speleothems are at oxygen isotopic equilibrium with drip water and their $\delta^{18}O$ values capture the surface-water oxygen isotopic signal. Aragonite-to-calcite transformation since the last glaciation is not noticeable in Furong stalagmites. Our multi-year field experiment approves that aragonite stalagmite $\delta^{18}O$ records in this cave are suitable for paleoclimate reconstruction. With high U, 0.5–7.2 ppm, and low Th, 20–1270 ppt, the Furong aragonite stalagmites provide very precise chronology (as good as ±20s yrs (2σ)) of the climatic variations since the last deglaciation. The synchroneity of Chinese stalagmite $\delta^{18}O$ records at the transition into the Bølling–Allerød (t-BA) and the Younger Dryas from Furong, Hulu and Dongge Caves supports the fidelity of the reconstructed East Asian monsoon evolution. However, the Furong record shows that the cold Older Dryas (OD) occurred at 14.0 thousand years ago, agreeing with Greenland ice core $\delta^{18}O$ records but ~200 yrs younger than that in the Hulu record. The OD age discrepancy between Chinese caves can be attributable to different regionally climatic/environmental conditions or chronological uncertainty of stalagmite proxy records, which is limited by changes in growth rate and subsampling intervals in absolute dating. Seasonal dissolved inorganic carbon $\delta^{13}C$ variations of 2–3‰ in the drip water and 5–7‰ in the pool and spring waters are likely attributed to variable degrees of CO_2 degassing in winter and summer. The variable $\delta^{13}C$ values of active deposits from −11‰ to 0‰ could be caused by kinetically mediated CO_2 degassing processes. The complicated nature of pre-deposition kinetic isotopic fractionation processes for

* Corresponding author. Tel.: +886 2 3366 5878, fax: +886 2 3365 1917.
E-mail address: river@ntw.edu.tw (C.-C. Shen).

0016-7037/$ - see front matter © 2011 Published by Elsevier Ltd.
doi:10.1016/j.gca.2011.04.003

carbon isotopes in speleothems at Furong Cave require further study before they can be interpreted in a paleoclimatic or paleoenvironmental context.

1. INTRODUCTION

Taking advantage of the absolute chronology possible with speleothems (e.g., Cheng et al., 2000; Shen et al., 2002; Richards and Dorale, 2003), such deposits have provided some of the most important environmental and climatic archives available today (e.g., Winograd et al., 1992; Dorale et al., 1998; Neff et al., 2001; Wang et al., 2001, 2004a; Yuan et al., 2004; Fairchild et al., 2006; Lachniet, 2009). Diverse geochemical and physical proxy records in speleothems on monthly-millennial time scales over different periods in the Quaternary have been reported (Bar-Matthews et al., 1997, 2003; Perrette et al., 2000; Tan et al., 2002; Fairchild et al., 2006; Baker et al., 2007; Affek et al., 2008; Wang et al., 2008; Cheng et al., 2009; Zhou et al., 2009; Shen et al., 2010). $\delta^{18}O$ and $\delta^{13}C$ have been the most commonly used proxies (e.g., Dorale et al., 1998; Wang et al., 2001, 2005, 2008; Bar-Matthews et al., 2003; Cheng et al., 2009; Tan et al., 2010). Despite complicated control factors and fractionation processes (e.g., Hendy, 1971; Lachniet, 2009; Dayem et al., 2010), stalagmite $\delta^{18}O$ has generally been accepted as a useful measure of precipitation in tropical and monsoonal regions (e.g., Wang et al., 2001, 2005, 2008; Yuan et al., 2004; Dykoski et al., 2005; Fleitmann et al., 2007; Frappier et al., 2007; Li et al., 2007; Wang et al., 2007; Cheng et al., 2009; Cruz et al., 2009; Li et al., 2011); while speleothem $\delta^{13}C$ records reflect regional vegetation trends (Dorale et al., 1998; Hellstrom et al., 1998; Bar-Matthews et al., 1996, 2003; Denniston et al., 2007).

Previous studies mainly focused on calcite stalagmites (e.g., Fairchild et al., 2006; Lachniet, 2009, and references therein). Long-term isotopic observations of oxygen and carbon in active speleothem calcite deposits and associated waters have also been monitored in different caves (e.g., Spötl et al., 2005; Treble et al., 2005; Johnson et al., 2006; Mattey et al., 2008). Aragonite speleothems can be deposited in caves formed in dolomitic host rocks (Hill and Forti, 1997) or under seasonal dry conditions (Railsback et al., 1994; Frisia et al., 2002). They have been used as archives for contemporary climate and environmental studies (e.g., Railsback et al., 1994; Finch et al., 2001, 2003; McMillan et al., 2005; Cosford et al., 2008). Aragonite-to-calcite transformation can occur in hundreds of years (Frisia et al., 2002) although the metastable aragonite can potentially exist in caves for thousands–millions of years (Fairchild et al., 2006). Oxygen and carbon isotopic signatures are possibly altered during phase transformations (e.g., Fairchild et al., 2006), and these can also induce a bias in their age determination (e.g., Ortega et al., 2005). Therefore, the applicability of fossil aragonite stalagmites to paleoclimate remains semi-quantitative (e.g., Frisia et al., 2002; Fairchild et al., 2006). Measurement of oxygen and carbon isotopic fractionations in aragonite speleothems and associated waters has been performed in only some European caves (e.g., McDermott et al., 1999; Frisia et al., 2000; McMillan et al., 2005), which limits their widespread applicability to the understanding of paleoclimate and paleoenvironment in different regions.

The evolution of the East Asian monsoon (EAM) has been revealed from stalagmite $\delta^{18}O$ records in Chinese caves, such as Hulu (Wang et al., 2001; Cheng et al., 2009), Dongge (Yuan et al., 2004; Wang et al., 2005), and Sanbao (Wang et al., 2008; Cheng et al., 2009). Systematic *in situ* monitoring programs and petrographic studies, however, have never been performed in these caves to give robust and direct evidence for supporting their application as a reflection of climatic conditions in the East Asian monsoon realm.

In this paper, a multi-year on-site monitoring program was performed at the Furong Cave, Chongqing, China. The characteristics of oxygen and carbon stable isotopic compositions in aragonite speleothems collected from the cave have been systematically addressed by comparing values recorded in active and inactive carbonates and in different water samples in and out of the cave. Carbonate and water data show that the mineralization of aragonite stalagmites occurs at oxygen isotopic equilibrium. Paleoclimate sequences recorded in the $\delta^{18}O$ proxy can be better constrained by this natural archive, with ppm-level uranium content. Agreement of stalagmite $\delta^{18}O$ sequences between Furong and Hulu/Dongge Caves (Wang et al., 2001; Yuan et al., 2004; Dykoski et al., 2005) since Termination I demonstrates their climatic application. The complicated natural dynamic of $\delta^{13}C$ in water and speleothem samples limits its direct application in paleoclimate reconstructions from Furong Cave.

2. SITE DESCRIPTION

Furong Cave (29°13′N, 107°54′E) is located in Cambrian dolomite rocks, on the east bank of Furongjiang River, a secondary branch of the Yangtze River, Chongqing, China (Fig. 1). The elevation at the entrance of Furong Cave is 480 m above sea level (asl) and 260 m above the Furongjiang River, with a main tunnel, 2–30 m in width and about 2800 m in length. The site features four huge halls, 30–50 m in height. Thickness of the covered soil mostly ranges from 0 to 30 cm. The upper vadose zone is 300–500 m thick. Chambers of this cave, were opened for tourism in 1994. An additional artificial tunnel, 180 m in length and 3 m in height, was excavated in 1998 (Fig. 2). The inner part of Furong Cave, ~50 m from the entrance, is well enclosed with 95–100% humidity. It has commonly been observed thus far that aragonite speleothems forms in cave passages cut in dolomite (Hill and Forti, 1997) and from parent waters with a relatively high Mg/Ca ratio (Morse et al., 1997). Formation of aragonite stalagmites in

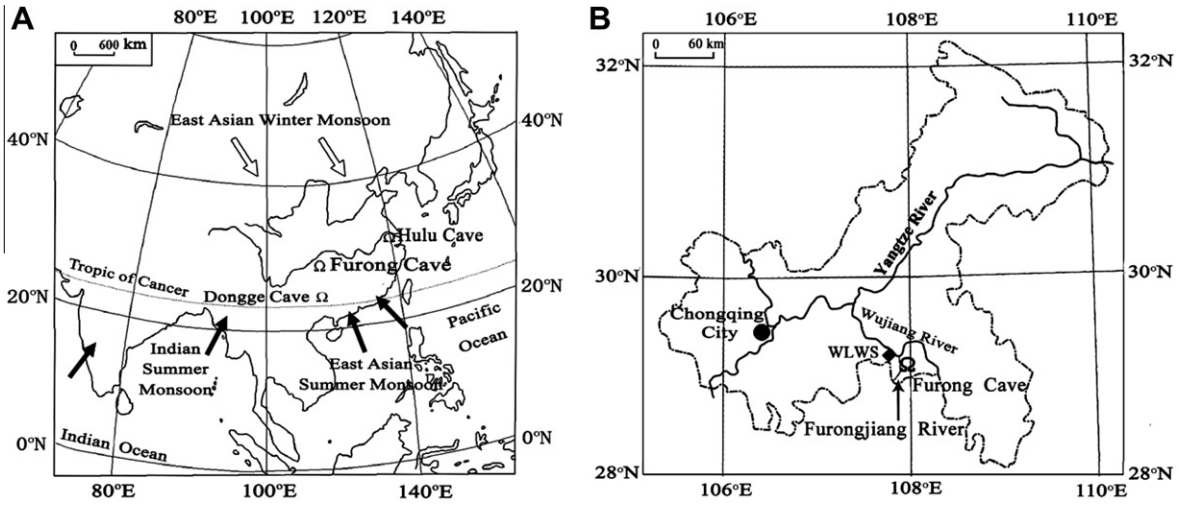

Fig. 1. Regional maps with Chinese caves. (A) Locations of Furong (29°13′N, 107°54′E), Hulu (32°30′N, 119°10′E) and Dongge (25°17′N, 108°05′E) Caves in the EAM realm. (B) Furong Cave is located near the Furongjiang River, 5 km from the Wujiang River and 20 km to the Wulong weather station (WLWS).

Furong Cave, which is cut in dolomite, is likely associated with the dolomite bedrock and high drip water Mg/Ca atomic ratios of 1–6 [monthly average from AD 2005 to 2009 at four water sampling sites in cave (Fig. 2)], determined by inductively coupled plasma optical emission spectrometry (ICP-OES) with 2σ reproducibility of ±2%.

The cave develops within a gorge and the karst with no snow cover is colonized by thick vegetation, mainly consisting of *Cinnamomum camphora* (Linn.) Presl., *Cinnamomum suavenium* Miq., *Lonicera mucronata* Rehd., *Loropetalum chinense* (R. Br.) Oliv., *Photinia serrulata* Lindl., and some shrubs. The height difference between the mountaintop and the river is ~1000 m (Fig. 2C). The regional climate is dominated by the EAM and characterized by two distinct seasons of cold–dry winter and hot–rainy summer. On average, the local annual precipitation is 1200 mm, with 70% of the rainfall in the wet season from May to October, typified by the year AD 2007 (Fig. 3A). In AD 2006 the cave site experienced a serious drought with total annual precipitation of 850 mm. Seasonal variations in the regional 29-month (April 2006–September 2008) precipitation $\delta^{18}O$ data show low values of $-15 \sim -12‰$ in summer and high values of $-4 \sim -2‰$ in winter (Li et al., 2010) (Fig. 3C).

3. MATERIAL AND EXPERIMENT

3.1. Cave temperature and air CO_2

Two automatic air temperature recorders were placed at drip water sampling sites #1 and #3 to monitor the cave air temperature every 2 h from November 2006–October 2007. These devices (StowAway TidbiT Temp Logger, Onset Computer Corporation model TBI32-20+50) have an operating range of −20 °C to 70 °C, accuracy of 0.2 °C with 0.02 °C resolution, and stability of 0.1 °C per year. Temperature values of drip water DW#1 and DW#3 were read monthly from November 2006 to July 2009, with WTW Multi 340i recorders with a measureable instrumental temperature range from −5 °C to 105 °C and an uncertainty of ±0.1 °C.

Monthly variations of air pCO_2 concentration at the same drip and pool water sampling sites (#1–#4) and one out-of-cave site, #5, 15 m from the artificial exit were monitored from March 2009 to July 2010, utilizing Testo 535 infrared CO_2 measuring instruments (Fig. 4). Detectable CO_2 concentrations range from 0 to 9999 ppmv and the precision is better than ±2% and accuracy is ±2% for 0–5000 ppmv CO_2.

3.2. Water samples

Monthly drip water samples (0.1–0.3 ml/drop), DW#1 and DW#3 (Fig. 2A) with drip rates of 100 and 70 drops/min, respectively, observed on October 21, 2006, and with drip heights of 22 m and 30 cm, respectively, from the ceiling in the Great Hall 30–50 m in height, were collected at sites #1 and #3, 1000 m from the natural entrance (Table 1 and Fig. 2A). Discharge of drip water DW#3 was monitored during March 2006–June 2007 (Fig. 3D). At sites #2 and #4, pool water samples, PW#2 and PW#4, were collected from two different pools, mainly supplied with drip water and seepage water from the vadose zone, with dimensions of 0.4 m (L) × 0.4 m (W) × variable depths of 0.2–0.4 m (D) and 3 m (L) × 2 m (W) × 0.4 m (D), respectively (Fig. 2A). Spring water sample SP#6, was collected from a site located above Furong Cave (Fig. 2B). Instantaneous water samples for measurements of $\delta^{18}O$ and dissolved inorganic carbon (DIC) $\delta^{13}C$ ($\delta^{13}C$-DIC), were collected monthly in two individual 50 ml polypropylene bottles over different periods, October 2005–June 2007 for DW#1, March 2006–June 2007 for DW#3, November 2005–June 2007 for PW#2 (no collection in September 2006), April 2006–June 2007 for PW#4, and March 2006–June 2007 for SP#6. For drip water, the bottles were placed on cleaned ground for 0.5–1 h sample collection. After carefully adding a 0.1-ml saturated $HgCl_2$ solution

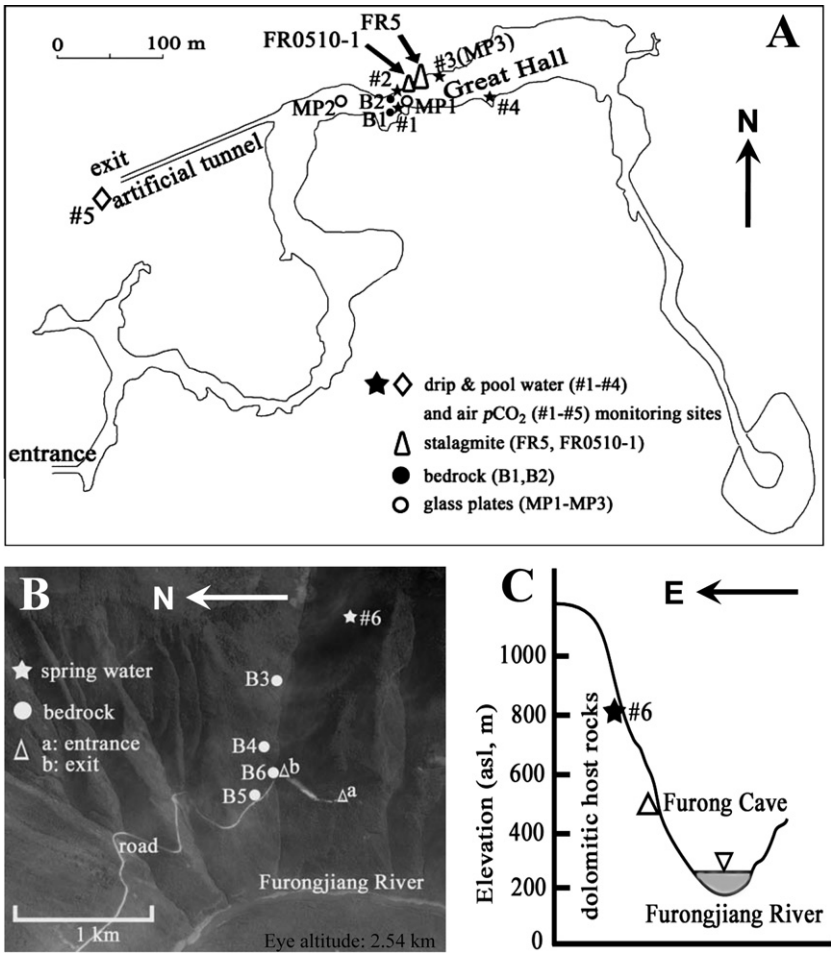

Fig. 2. (A) Sketch of Furong Cave. Monthly drip water samples, #1 and #3, and pool water samples, #2 and #4, (stars) were collected from 2005 to 2007. Air pCO_2 were monitored at sites #1–#5 (stars and diamond) from March 2009 to July 2010. Glass plate carbonates, MP1–MP3 (hollow circles), and two bedrock samples, B1 and B2 (solid circles), were collected in the Great Hall. Two active stalagmite, FR0510-1 (small triangle), and FR5 (large triangle), were also collected in the chamber. (B) An aerial view of Furong Cave bedrock and Furongjiang River (from Google Earth). The entrance and artificial exit of the cave are labeled as "a" and "b", respectively. Four bedrock samples, B3, B4, B5, and B6, were hammered. Monthly spring water samples were taken at site #6. (C) An altitudinal sketch map with the entrance of Furong Cave (hollow triangle), host rock, spring water site (star) and Furongjiang River (gray area).

to the collected drip and pool water samples to avoid microbial isotopic fractionation, the bottles were sealed in cave. They were then stored at 5 °C in laboratory, followed by chemistry and instrumental analysis in 1–3 days.

3.3. Carbonate samples

Pristine bedrock samples, ~200 g each, were hammered and active deposits, 0.3–1 mm in thickness and 0.1 g in weight, growing with drip water or in pool water, were scraped from the surface on November 24, 2005 (Fig. 2 and Table 2). The collected active speleothems are samples of accreting surfaces of soda straws and stalagmites, crystals in pool water, flowstone, and a soda straw growing in the artificial tunnel (Table 2). Sample A1, white calcium carbonate, has been depositing on the ceiling of the artificial exit tunnel since 1998. The other active deposits were taken from the Great Hall (Table 2).

Three circular glass plates, 9 cm in diameter, were placed under active drip sites, MP1, MP2, and MP3, with 7-month (December 2009–June 2010) averaged discharge of 30 ± 8 ml/min, 18 ± 7 ml/min, and 7 ± 1 ml/min, respectively, in the Great Hall to form modern deposits. The glass plate speleothems, growing from December 28, 2007 to September 24, 2008, were collected for determination of morphological composition using a polarizing microscope, ECLIPSE Nikon E600W POL, and for C/O isotope equilibrium precipitation test.

Two active stalagmites, FR0510-1, 7.3 cm in length with a diameter of about 5 cm, and FR5, 50 cm in length with a variable diameter of 6 cm at the top and 14 cm at the bottom (Fig. 5), were collected in the Great Hall in October and May 2005, respectively (Fig. 2A). The X-ray diffraction analyses on powdered subsamples collected from the top (0–0.5 mm) and bottom (7–7.5 mm) of FR0510-1 and from depths of 2.5, 15.5, and 30.5 mm of FR5 show that the two

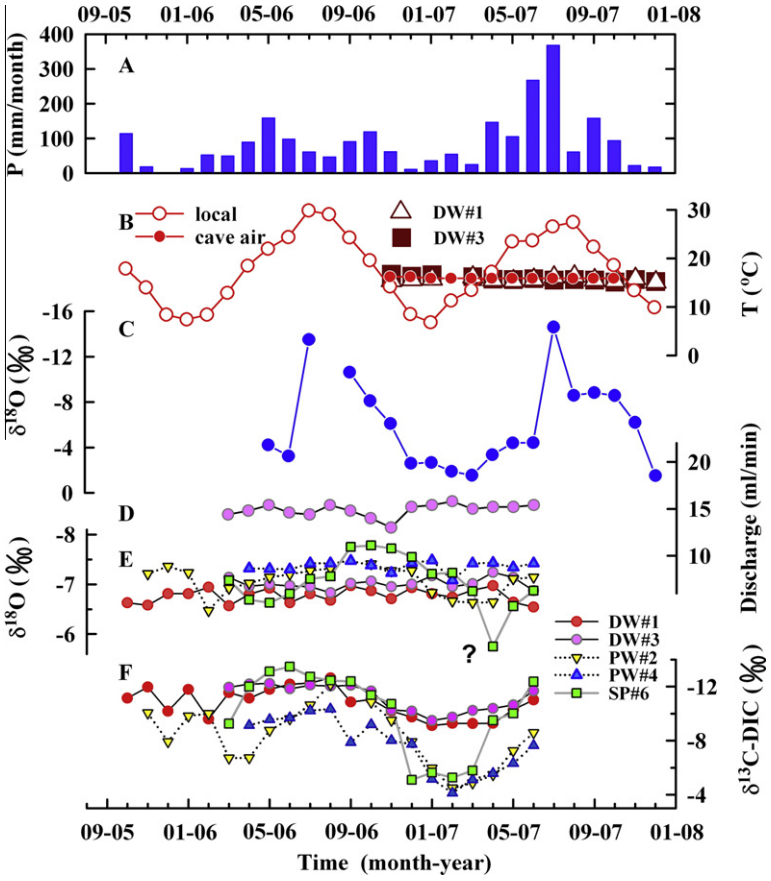

Fig. 3. (A) Local precipitation (bars). (B) Temperatures of local air (hollow circles), cave air (solid circles), drip water samples DW#1 (triangles) and DW#3 (squares). (C) Monthly regional rainwater $\delta^{18}O$ (circles) (Li et al., 2010). (D) Discharge of drip water sample DW#3. (E) $\delta^{18}O$ and (F) $\delta^{13}C$-DIC of drip water (circles, solid lines), pool water (triangles, dashed lines), and spring water (squares, gray line) samples. Note that there is an elusive high value of −5.8‰ for drip water $\delta^{18}O$ in April 2007.

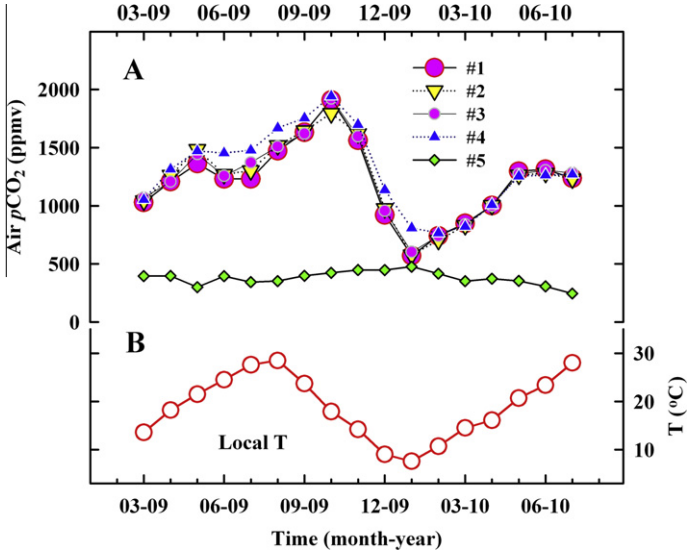

Fig. 4. (A) Air pCO_2 at four in-cave sites #1–#4 and one out-of-cave site #5 and (B) local air temperature from March 2009 to July 2010.

stalagmites are pure aragonite with no detectable calcite (<3%; Li et al., 2011). To further carefully evaluate possible aragonite-to-calcite transformation for the two stalagmites, the *in situ* (0.5 cm × 0.5 cm) mineral compositions and

Table 1
$\delta^{18}O$ and $\delta^{13}C$-DIC data for samples of drip water, pool water and spring water.

Samples	Mean $\delta^{13}C$-DIC[a] (‰)	$\pm1\sigma$	Mean $\delta^{18}O$[a] (‰)	$\pm1\sigma$	Monitoring course (months)
Drip water (DW#1)	−10.78	1.12	−6.77	0.14	21
Pool water (PW#2)	−8.28	2.19	−7.06	0.28	19
Drip water (DW#3)	−11.17	0.99	−7.02	0.11	16
Pool water (PW#4)	−7.71	2.02	−7.36	0.11	15
Spring water (SP#6)	−10.08	3.03	−7.05	0.53	16

[a] Averaged monthly values during the individual monitoring courses. Detailed records are illustrated in Fig. 4.

Table 2
$\delta^{18}O$ and $\delta^{13}C$ data of bedrock carbonate samples (B1–B6) and active deposits (others).

Sample ID	$\delta^{13}C$ (‰)	$\delta^{18}O$ (‰)	Sample location	Note
B1	0.75	−8.19	3 m to site #1 in cave	
B2	0.07	−10.08	2 m to site #2 in cave	
B3	−1.52	−9.48	Mountainside	
B4	−2.62	−11.46	Mountainside	
B5	−1.85	−8.36	By the road, 200 m to cave exit	
B6	−1.69	−9.89	Cave exit	
A1	−11.43	−7.23	Ceiling of the exit tunnel	Deposit since 1998
A2	−0.13	−6.38	1 m to site #2	Deposit on the top of an active stalagmite
A3	−10.03	−6.73	Site #1	Deposit with drip water from a 22-m height
A4	−8.55	−6.54	2 m to site #1	White deposit on the top of a stalagmite
A5	−8.02	−6.70	4 m to site #1	Deposit on a broken rock
A6	−5.67	−6.80	1 m to site #3	Tip of an active soda straw
A7	−10.67	−7.43	Vertically under site #3	Active tooth-like crystal
A8	−4.16	−6.94	In the Great Hall	Active stalagmite deposit
A9	−7.16	−6.60	10 m to site #4	Deposit on the top of an active stalagmite
A10	−4.2	−5.86	Flowstone near #4 site	Active flowstone with dripping water
A11	−5.62	−6.56	9 m to site #3	Stalagmite deposit since AD 1996
A12	−1.37	−6.51	10 m to site #3	Deposit on the top of an active stalagmite
A13	−4.22	−6.61	In the pool of site #4	Active crystal in pool water

polymorphs at depth 5.2 cm of FR0510-1 and depths of 11, 12, and 22 cm of FR5 were scanned using electron backscatter diffraction (EBSD) techniques (McMillan et al., 2005; Neuser and Richter, 2007) by a scanning electron microscope (SEM), FEI-QUANTA 200 FEG, with 3–5-μm spatial resolution.

3.4. ^{230}Th dating and oxygen/carbon stable isotopic and ^{14}C analyses

^{230}Th dating was performed in the High-Precision Mass Spectrometry and Environment Change Laboratory (HISPEC), National Taiwan University. Fourteen subsamples, 1 mm in width and 50–200 mg in weight, were drilled from a flat polished surface along the deposit lamina on the stalagmite FR5 for U–Th chemistry (Shen et al., 2003) and isotopic measurements were made using a multi-collector inductively coupled plasma mass spectrometer (MC-ICP-MS), Thermo Electron Neptune (Frohlich et al., 2009; Shen et al., 2010).

The subsampling process was performed on a class-100 clean bench in a class 10,000 clean room to avoid possible contamination (Shen et al., 2008). A triple-spike, ^{229}Th–^{233}U–^{236}U, isotope dilution method was employed to correct mass bias and determine uranium concentrations (Shen et al., 2003). A protocol, using one newly-developed MasCom secondary electron multiplier with repelling potential quadrupole was employed. No significant difference between measurements of standards carbonate samples on an ICP-sector-field-MS (ICP-SF-MS; Shen et al., 2002) and on the MC-ICP-MS certify the MC-ICP-MS methodology (Frohlich et al., 2009; Shen et al., 2010). Off-line calculations of U–Th isotopic data (Table 3) and ^{230}Th dates (yr BP, before AD 1950) were described in Shen et al. (2002, 2008). Precisions of the corrected ^{230}Th dates range from ±24–59 yrs (2σ), except for the subsample FR5-13 at depth 185 mm (±81 yrs). ^{232}Th levels are from 20 to 1270 ppt (Table 3). Corrections for initial ^{230}Th correspond to only 0–15 yrs, smaller than dating error. The chronology of the stalagmite is established using linear interpolation between ^{230}Th dates, which are in stratigraphic order. For the stalagmite FR0510-1, depths of 4, 20, 35, 49, and 63 mm, have been ^{230}Th-dated by Li et al. (2011).

Subsamples, ~50 μg each, for carbon and oxygen stable isotope analyses of FR5 were drilled at 0.5–1-mm intervals, corresponding to an averaged temporal resolution of 30 yrs, along the growth axis of the stalagmite. One additional top

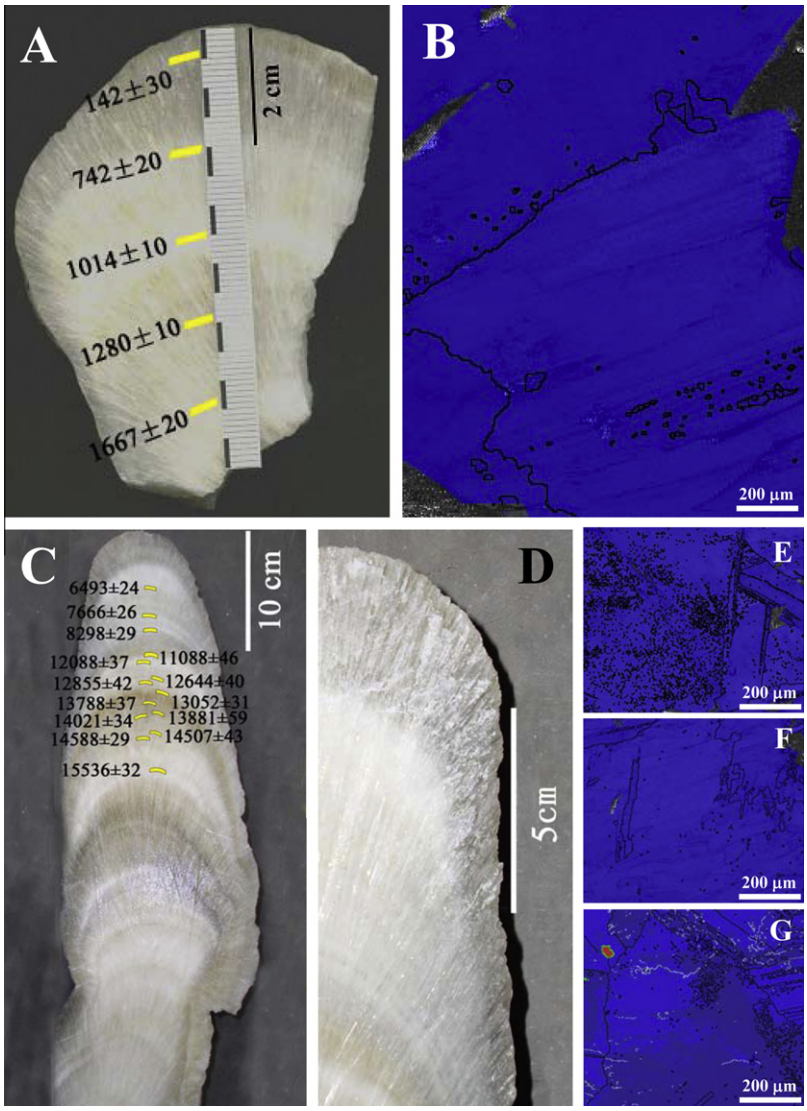

Fig. 5. (A) A photograph of active aragonite stalagmite FR0510-1, collected in October, 2005, with ^{230}Th dates (data from Li et al., 2011). (B) An EBSD image of FR0501-1 at depth 5.2 cm expressing 100% aragonite (blue). (C) A photograph of stalagmite FR5 with ^{230}Th dates, (D) its enlarged upper 13-cm section, and EBSD images at depths of (E) 11 cm, (F) 12 cm, and (G) 22 cm. The polymorph-unidentifiable area is shown in gray. Green lines are phase boundaries. White and black curves denote crystal boundaries with misorientation angles smaller and larger than 20°, respectively. At depth 22 cm of FR5 showing 100% aragonite (blue) with 0.013% intrusive calcite (orange).

subsample, FR5-top, 0–0.10 mm in depth, was carefully scraped. Seven coeval subsamples drilled from different fabrics on five laminae, at 90, 120, 210, 290 and 415 mm from top, of stalagmite FR5 were drilled for the Hendy Test (Hendy, 1971).

Oxygen and carbon stable isotopic compositions in the carbonate samples were measured on a Finnigan Delta V Plus gas isotope mass spectrometer, combined with a Kiel IV automated carbonate device at the Laboratory of Geochemistry and Isotope, School of Geographical Sciences, Southwest University, Chongqing. The international standard NBS19 and laboratory standards NCKU1 and SWU1 were measured between every 5 and 7 samples, with a long-term 1σ precision of 0.1‰ for δ^{18}O and 0.06‰ for δ^{13}C. Water δ^{18}O and δ^{13}C-DIC were analyzed on the Delta V plus combined with a Gas Bench automated device. The 1σ external precision is 0.15‰ for δ^{18}O and 0.1‰ for DIC δ^{13}C. Values are reported as δ^{18}O (‰) with respect to the Vienna Pee Dee Belemnite (VPDB) standard for carbonate and to the Vienna Standard Mean Ocean Water (VSMOW) for water. δ^{13}C-DIC and carbonate δ^{13}C data are reported relative to the VPDB standard. All δ^{18}O and δ^{13}C uncertainties in this paper are one standard deviation (1σ) unless otherwise noted.

To evaluate the temporal contribution of bedrock carbon to the speleothem-depositing seepage water, 0.2-mg subsamples were drilled at depths of 0.5, 4.0, 20.0, 35.0, 49, and 63.0 mm from stalagmite FR0510-1 for ^{14}C accelerator mass spectrometric (AMS) analyses at the State Key

Table 3
U–Th isotopic data and ^{230}Th ages for subsamples of stalagmite FR5 by MC-ICP-MS at the HISPEC, National Taiwan University.

Sample ID	Depth (mm)	^{238}U (ppb)	^{232}Th (ppt)	$\delta^{234}U_{measured}$[a]	$[^{230}Th/^{238}U]_{activity}$[c]	$[^{230}Th/^{232}Th]$[d] (ppm)	Age (yr) uncorrected	Age (yr BP) corrected[c,e]	$\delta^{234}U_{initial}$ corrected[b]
FR5-1	57	487 ± 1	1270 ± 4	3704 ± 5	0.2765 ± 0.0009	1750 ± 8	6566 ± 23	6494 ± 24	3773 ± 5
FR5-2	80.5	499.6 ± 0.5	852 ± 4	4192 ± 5	0.3581 ± 0.0011	3466 ± 19	7732 ± 26	7667 ± 26	4285 ± 5
FR5-3	89.5	421.9 ± 0.2	24 ± 16	4096 ± 3	0.3790 ± 0.0013	106,908 ± 70,589	8356 ± 29	8298 ± 29	4194 ± 3
FR5-4	109.5	988 ± 2	78 ± 13	3808 ± 12	0.4724 ± 0.0015	99,096 ± 17,123	11,146 ± 46	11,088 ± 46	3930 ± 12
FR5-5	111.5	1072 ± 1	484 ± 3	3528 ± 5	0.4831 ± 0.0013	17,657 ± 122	12,149 ± 37	12,089 ± 37	3651 ± 6
FR5-6	128	1836 ± 2	819 ± 4	3732 ± 6	0.5278 ± 0.0014	19,527 ± 103	12,724 ± 40	12,665 ± 40	3868 ± 6
FR5-7	130.5	1201 ± 2	49 ± 13	3789 ± 8	0.5418 ± 0.0014	220,054 ± 60,820	12,913 ± 42	12,855 ± 42	3930 ± 8
FR5-8	135	3793 ± 3	20 ± 4	3754 ± 6	0.5456 ± 0.0011	12,37,803 ± 297,700	13,110 ± 31	13,051 ± 31	3896 ± 6
FR5-9	150	2744 ± 3	65 ± 4	3619 ± 6	0.5585 ± 0.0012	387,011 ± 29,018	13,846 ± 37	13,787 ± 37	3764 ± 6
FR5-10	155	3100 ± 7	82 ± 4	3547 ± 12	0.5532 ± 0.0017	343,694 ± 16,422	13,939 ± 59	13,881 ± 59	3689 ± 13
FR5-11	157	2420 ± 2	47 ± 5	3476 ± 5	0.5497 ± 0.0011	470,189 ± 48,872	14,080 ± 35	14,021 ± 34	3617 ± 6
FR5-12	169	5091 ± 7	839 ± 4	3489 ± 6	0.5694 ± 0.0014	57,059 ± 274	14,566 ± 43	14,508 ± 43	3635 ± 6
FR5-13	170.5	5232 ± 4	45 ± 12	3489 ± 4	0.5725 ± 0.0010	11,08,850 ± 313,580	14,646 ± 29	14,588 ± 29	3637 ± 4
FR5-14	179	4351 ± 5	47 ± 6	3550 ± 6	0.5956 ± 0.0012	904,021 ± 104,227	15,055 ± 37	14,996 ± 37	3704 ± 6
FR5-15	185	7201 ± 20	278 ± 6	3612 ± 15	0.607 ± 0.002	259,394 ± 5744	15,128 ± 81	15,070 ± 81	3770 ± 15
FR5-16	201.5	6628 ± 5	37 ± 11	3647 ± 4	0.6290 ± 0.0011	18,83,737 ± 582,588	15,594 ± 32	15,536 ± 32	3812 ± 5

Analytical errors are 2σ of the mean.

[a] $\delta^{234}U = ([^{234}U/^{238}U]_{activity} - 1) \times 1000$.

[b] $\delta^{234}U_{initial}$ corrected was calculated based on ^{230}Th age (T), i.e., $\delta^{234}U_{initial} = \delta^{234}U_{measured} \times e^{\lambda_{234} * T}$ and T is corrected age.

[c] $[^{230}Th/^{238}U]_{activity} = 1 - e^{-\lambda_{230}T} + (\delta^{234}U_{measured}/1000)[\lambda_{230}/(\lambda_{230} - \lambda_{234})](1 - e^{-(\lambda_{230}-\lambda_{234})T})$, where T is the age. Decay constants are 9.1577×10^{-6} yr^{-1} for ^{230}Th, 2.8263×10^{-6} yr^{-1} for ^{234}U (Cheng et al., 2000), and 1.55125×10^{-10} yr^{-1} for ^{238}U (Jaffey et al., 1971).

[d] The degree of detrital ^{230}Th contamination is indicated by the $[^{230}Th/^{232}Th]$ atomic ratio instead of the activity ratio.

[e] Age (before AD 1950) corrections were calculated using an estimated $^{230}Th/^{232}Th$ atomic ratio of 4 ± 2 ppm, which is the value for a material at secular equilibrium with the crustal $^{232}Th/^{238}U$ value of 3.8 and an arbitrarily uncertainty of 50%.

Laboratory of Nuclear Physics and Technology, Peking University, Beijing (Liu et al., 2007).

4. RESULTS AND DISCUSSION

4.1. Monthly temperature records

The averaged monthly cave drip water temperature is 15.7 ± 0.5 °C at sites #1 and #3 in the Great Hall, which agrees with the measured cave air temperature, in the range of 16.0–16.3 °C from November 2006 to October 2007 (Fig. 3B). The cave thermal condition reflects the annual mean regional air temperature of 16.4 ± 0.3 °C, inferred from an averaged temperature of 18.0 ± 0.3 °C during 2005–2009 recorded at Wulong weather station, 20 km away from and 250 m lower in elevation than Furong Cave (Fig. 3B), and a lapse slope of 0.65 °C per 100 m in Chongqing (Dan et al., 2008).

4.2. Water $\delta^{18}O$

Monthly $\delta^{18}O$ records of water samples from 2005 to 2007 are plotted in Fig. 3E and the long-term averages are given in Table 1. The 16-month spring water SP#6 $\delta^{18}O$ data changed from high values of $\sim -6.5‰$ in April–May 2006 to low values of $\sim -7.5‰$ in September–December 2006, experienced an anomalous high value at $-5.8‰$ in April 2007, and then shifted to $-6.6 \sim -6.9‰$ (Fig. 3E).

Comparison with rainfall $\delta^{18}O$ with seasonal variability of $\sim 10‰$, the spring water $\delta^{18}O$ has the same annual $\delta^{18}O$ mean of $-7.1‰$ and dampened seasonal change of only $1‰$ (except for the elusive value in April 2007). The evidences indicate mixing of rainfall and seepage water in the upper 400-m thick bedrock (Fig. 2). An observed 3-month lag between spring water $\delta^{18}O$ and rainfall records implies multimodal flow through conduits and fractures feeding the spring water pool.

The $\delta^{18}O$ results from three of the four drip and pool water samples, DW#1, DW#3, and PW#4, do not show evidence of a clear seasonal cycle (Fig. 3E). One-sigma $\delta^{18}O$ variations are only ± 0.11–$0.28‰$ (Table 1). The $\delta^{18}O$ of pool water PW#2 exhibits a slight variability of $\pm 0.28‰$, larger than $\pm 0.11‰$ for the pool water PW#4, likely caused by variable water supply year-round in this small water pool at site #2 with variable depths of 0.2–0.4 m and a reservoir volume of only 0.032–0.064 m^3. Instead, lack of seasonal water $\delta^{18}O$ change is observed for the PW#4 with steady water supply and relative large water volume of ~ 2.4 m^3. An averaged pool water PW#4 $\delta^{18}O$ of $-7.36 \pm 0.03‰$ (1σ of the mean, $1\sigma_m$) is slightly lower than those for PW#2 ($-7.06 \pm 0.07‰$) and drip water (Table 1), which implies less evaporation occurring through the pathway for this pool water.

The drip water $\delta^{18}O$ values at two collection sites, $-6.77 \pm 0.14‰$ for #1 and $-7.02 \pm 0.11‰$ for #3, are consistent with the annual mean regional rainfall $\delta^{18}O$ value of $-7.1‰$ (Student's t-test, $p = 0.05$), suggesting that the oxygen isotopic composition of the supplying water into the cave reflects an averaged rainfall condition. The absence of oxygen isotope shifts over different seasons shows a thorough mixing and long-term storage of waters in a karst aquifer with seepage-fed flow at the sites (Fairchild et al., 2006).

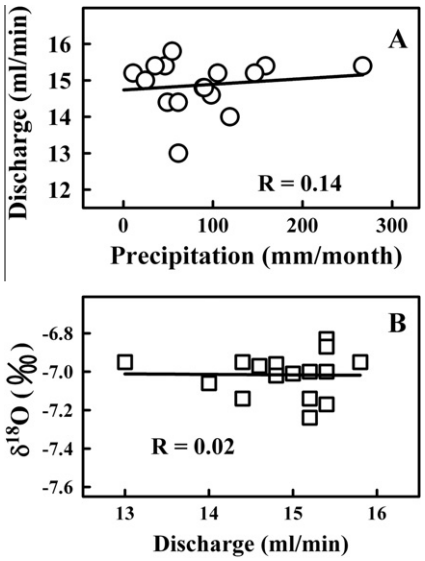

Fig. 6. Plots of (A) discharge of drip water DW#3 versus local precipitation and (B) $\delta^{18}O$ versus discharge for drip water DW#3.

The drip water rate or discharge in Furong Cave is different from those, strongly correlated with seasonal rainfall in Grotta di Ernesto Cave in NE Italy (Miorandi et al., 2010) and Heshang Cave in Hubei Province, China (Johnson et al., 2006) with annually banded stalagmites. The steady monthly drip water discharge of 13–16 ml/min in Furong Cave (Fig. 3D) is similar to the observations at site PH1 in Obir Caves, Northern Karawanken Mountains, Austria (Spötl et al., 2005) and sites in DeSoto Caverns, central Alabama, SE USA (Lambert and Aharon, 2011). With additional evidences of poor correlations between drip water discharge and precipitation ($R = 0.14$) and between drip water $\delta^{18}O$ and discharge ($R = 0.02$) at site DW#3 (Fig. 6) and also no any annually laminated stalagmites found in Furong Cave, it suggests that the residence time of drip water in the vadose zone of the Great Hall could be longer than 1 yr. The infiltrating rainwater was homogenized in the zone and monthly variability of water $\delta^{18}O$ was suppressed. Hence the cave drip water oxygen isotopic composition is interpreted here as an annual rainfall $\delta^{18}O$ signal.

4.3. Water $\delta^{13}C$-DIC

The $\delta^{13}C$-DIC data of drip water, pool water and spring water samples are plotted in Fig. 3F. The averaged values and 1σ monthly deviations are listed in Table 1. The spring water SP#6 out of the cave is characterized by $\delta^{13}C$-DIC extremes of $-12‰$ to $-13‰$ in summer and $-5‰$ to $-6‰$ in winter. These are in phase with wet and dry climatic seasons (Fig. 3), suggesting variability of soil CO_2 production is an important factor. The timing of the enriched $\delta^{13}C$-DIC values is consistent with the low precipitation rate of 10–50 mm/month during December 2006–

March 2007. Using an isotopic fractionation of ~10‰ between CO_2 gas and bicarbonate ion in water (Hendy, 1971; Dulinski and Rozanski, 1990; Lambert and Aharon, 2011), a $\delta^{13}C$ value of −22‰ to −23‰ or less is inferred for the soil atmospheric CO_2. The light $\delta^{13}C$ in wet season was likely derived from vigorous photosynthetic processes of the local dominant C_3 vegetation (Hendy, 1971; McDermott, 2004, and references therein).

Seasonal $\delta^{13}C$-DIC variability of pool water is from −12‰ to −5‰ for PW#2 and from −10‰ to −5‰ for PW#4 (Fig. 3F). The only exceptions are the PW#2 samples collected from November 2005–February 2006, which show a weak trend unrelated to seasonality. The amplitude of seasonal water $\delta^{13}C$-DIC change in pool #2 is 2‰ larger than that in pool #4. These two cases could be attributed to a small reservoir volume of 0.032–0.064 m^3 for pool #2 with variable water supply and aqueous CO_2 degassing.

Similar to pool water, drip water is characterized by seasonal $\delta^{13}C$-DIC changes of 2–3‰, from −12‰ in April–September of 2006 to −9‰ ~ −10‰ between December of 2006 and April of 2007. The small seasonal change of drip water $\delta^{13}C$-DIC at site #1 and #3 is only one-third of the observed pool water values of 5–7‰, likely resulting from (1) a long residence time (>1 yr) of drip water in the vadose zone (Section 4.2), (2) an isotopic equilibrium between soil CO_2 and water with depth below only 30 cm (Breecker et al., 2009), and (3) a relatively short degassing time interval. The consistency of the two drip water $\delta^{13}C$-DIC records is apparently independent of various drip rates or drip heights (see Section 3.2). This indicates that the fractionation of drip water DIC $^{13}C/^{12}C$ and degree of degassing should be associated with different processes.

Cave air pCO_2 presents notable seasonal variability in Furong Cave (Fig. 4). The concurrent high air pCO_2 levels of four sites, #1–#4, in the Great Hall (Fig. 2), range from 1200 to 1900 ppmv in summer during the monitoring period from March 2009 to July 2010. The low values of cave air pCO_2 were about 570–800 ppmv in winter (Fig. 4).

Seasonal variation of drip water $\delta^{13}C$-DIC in Furong Cave is similar to that in DeSoto Caverns (Lambert and Aharon, 2011). The air pCO_2 and isotopic records of drip water $\delta^{18}O$ and $\delta^{13}C$-DIC also resemble those in the Obir Caves (Spötl et al., 2005). The coincidence suggests a similar kinetically-enhanced process probably operating in Furong Cave. A seasonally changing air flow results in high summer pCO_2 and low winter pCO_2 in the Obir Caves. Unlike summer conditions, the cold CO_2-poor air, drawn into the cave through the entrance in winter, enhances degassing of water CO_2 and causes concomitant ^{13}C-enriched carbonate deposition in the Obir Caves (Spötl et al., 2005). Frisia et al. (2011) have also carefully demonstrated the effect of kinetic degassing on drip water $\delta^{13}C$-DIC value. The seasonal change of 5–7‰ in the pool water $\delta^{13}C$-DIC in Furong Cave might be attributed to this kinetic process. The relatively immobile pool water experiences longer exposure times, with enhancement of degassing of water CO_2, resulting in a ~10‰ increase in ^{13}C (e.g., Hendy, 1971; Spötl et al., 2005). This results in substantially larger seasonal DIC carbon isotopic changes in pool water, as compared with drip water.

4.4. $\delta^{18}O$ and $\delta^{13}C$ of bedrocks and active speleothems

4.4.1. Bedrock

The $\delta^{18}O$ and $\delta^{13}C$ contents of bedrock samples, two in-cave samples and four out-of-cave samples (Fig. 2) range from −11.5‰ to −8.2‰ and from −2.6‰ to 0.1‰, respectively (Table 2). The oxygen and carbon isotopic compositions are consistent with values of the Cambrian dolomites in the Argentine Precordillera (Buggisch et al., 2003). The data also match $\delta^{18}O$ values, from −11‰ to −7‰, and $\delta^{13}C$, from −2‰ to 1‰, of Cambrian marine calcitic shells (Veizer et al., 1999). The $\delta^{18}O$ and $\delta^{13}C$ values of the bedrock around Furong Cave might be from marine biological origin during Cambrian.

4.4.2. Active speleothems

Isotopic results from 13 active speleothems, collected from the top of active stalagmites with drip water, surface of flowstones and tip of soda straw, are given in Table 2. The $\delta^{18}O$ values range from −7.4‰ to −5.9‰ and the $\delta^{13}C$ values from −11.4‰ to −0.1‰. The $\delta^{18}O$ mean and 1σ variation are -6.68 ± 0.39‰ for all active deposits, including flow stone, stalactites and stalagmites from the artificial exit tunnel and inner chamber. For stalagmite deposits in the inner chamber, including A2, A4, A5, A8, A9, A11 and A12, the averaged $\delta^{18}O$ value is -6.60 ± 0.18‰, slightly larger than the instrumental uncertainty of ±0.10‰, suggesting additional factors involved. The $\delta^{18}O$ value of −6.38‰ for a 0.3-mm top deposit of A2 is not distinguishable from those of −6.28‰ for the top 0.25 mm (~13 yrs, AD 1993–2005; Li et al., 2011) of FR0510–1 and −6.38‰ for the top 0.10 mm (~22 yrs, AD 1983–2005) of FR5. The more depleted $\delta^{18}O$ values, such as −6.94‰ for A9 and −6.70‰ for A5 (Table 2), also indicate additional factors involved. They can be attributed to different dissolution of bedrock (Section 4.5) with low $\delta^{18}O$ of −11.5‰ to −8.2‰ (Table 2) through conduits and fractures in the vadose zone. Another possibility is that the scarped subsamples contain deposits older than 50 yrs with $\delta^{18}O$ values of −6.9 ~ −6.6‰ (Fig. 7 of Li et al., 2011).

The $\delta^{13}C$ values of active speleothems vary from −0.1‰ to −11.4‰, with an average of -6.2 ± 3.5‰. For stalagmite

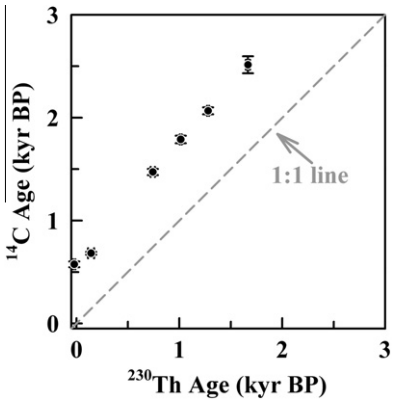

Fig. 7. A plot of calibrated ^{14}C age [IntCal09 (Reimer et al., 2009)] versus ^{230}Th age for six layers of stalagmite FR0510-1.

deposits only, the $\delta^{13}C$ value is $-5.0 \pm 3.3‰$. The notable $\delta^{13}C$ variability is similar to that in Stump Cross Caverns, Yorkshire, England (Baker et al., 1997). Baker et al. (1997) proposed three possible mechanisms to explain such a wide range of values: (1) disequilibrium with soil CO_2, (2) degassing of groundwater within the unsaturated zone, and (3) CO_2 degassing during the deposition process. Compared to the large ± 3–$4‰$ variation and elevated $\delta^{13}C$ values in the active cave deposits, the $\pm 1‰$ seasonal $\delta^{13}C$-DIC variation of drip water is small (Fig. 3F and Table 1). This suggests that the first two processes are unlikely to account for the ^{13}C fractionation at the Furong site and CO_2 degassing remains as the most possible candidate.

Model results suggest that speleothem $^{13}C/^{12}C$ kinetic fractionation is dependent on temperature, isotopic composition of the initial solution, and the time elapsed since degassing commenced (Dulinski and Rozanski, 1990). In Furong Cave, the drip water temperature is stable year-round (Fig. 3B), which cannot result in the wide range of active deposit $\delta^{13}C$ from $0‰$ to $-11‰$. The $\delta^{13}C$-DIC of drip water varies slightly, only $\pm 1‰$, suggesting an insignificant or minor CO_2 degassing of groundwater within the aquifer before reaching the cave void. The elevated $^{13}C/^{12}C$ ratios recorded in active speleothems from the DIC values of $-11 \pm 1‰$ in drip water is most likely attributed to a kinetic fractionation process during precipitation. Carbonate $\delta^{13}C$ can be elevated $10‰$ after degassing over a 10 min period at the onset of precipitation (Dulinski and Rozanski, 1990; Baker et al., 1997). In addition, the large seasonal range of over 1000 ppmv for cave air pCO_2 (Fig. 4) can cause different $\delta^{13}C$-DIC changes in cave waters (Fig. 3F) and variable kinetically enhanced CO_2 degassing processes in Furong Cave, resulting in a wide $\delta^{13}C$ range of 11–$12‰$ in active speleothems (Table 2).

4.5. Contribution of bedrock carbon to seepage water and speleothem

Frisia et al. (2011) have shown a significant contribution of bedrock carbon to the drip water DIC in Grotta di Ernesto Cave, NE Italy. A plot of calibrated ^{14}C age versus ^{230}Th age (Li et al., 2011) for stalagmite FR0510-1 is given in Fig. 7, which is used to evaluate the contribution of bedrock carbon to seepage water and speleothem. The mean ^{14}C age offset from ^{230}Th age is 710 ± 240 yrs. The primary source of speleothem-depositing drip water DIC is soil CO_2 from plant root respiration and decomposition of organic matter and another source is dissolution of bedrock carbonate (Hendy, 1971). The dead carbon proportion (DCP) of seepage water is, therefore, attributed to bedrock carbonate dissolution with negligible ^{14}C and aging of soil organic matter (Genty et al., 2001). Over the past 1.67 kyrs, the DCP on the six arbitrarily selected layers of the stalagmite is 7–9%, calculated by Eqs. (1) and (2) of Genty et al. (2001). The covered soil at Furong mostly ranges from 0 to 30 cm layer and the source of organic matter decay to DCP should be limited. This DCP can be considered as the contribution at most from bedrock to the drip water DIC.

4.6. Oxygen isotopic fractionation between active speleothem and water

For speleothem stable isotopes, deposition at equilibrium is an important premise for paleoclimate applications. Evaluation of $^{18}O/^{16}O$ equilibrium fractionation of aragonite, however, is impeded by diverse aragonite $\delta^{18}O$-water $\delta^{18}O$-temperture equations (e.g., McCrea, 1950; Grossman and Ku, 1986; Patterson et al., 1993; Thorrold et al., 1997; Zheng, 1999; Böhm et al., 2000; Zhou and Zheng, 2003; Kim et al., 2007). The discrepancies among aragonite $\delta^{18}O$-water-temperature equations are likely attributed to the different experimental conditions (Kim et al., 2007). Zheng (1999) and Zhou and Zheng (2003) calculated the equations by inorganically precipitated aragonite, while McConnaughey (1989), Thorrold et al. (1997) and Böhm et al. (2000) determined the oxygen fractionation between aragonite and water with shallow-water coral, marine fish otolith and coralline sponge, respectively. Lachniet (2009) reviewed available expressions in the literature and recommended an experimental aragonite–water fractionation equation at equilibrium conditions (Kim et al., 2007):

$$1000 \ln \alpha = 17.88\ (\pm 0.13) \times 1000/T - 31.14\ (\pm 0.46) \quad (1)$$

where α indicates the $^{18}O/^{16}O$ fractionation between aragonite and water and T is depositional temperature in Kelvin (K). This equation is very similar to the one derived from fish otolith aragonite (Patterson et al., 1993):

$$1000 \ln \alpha = 18.56\ (\pm 0.32) \times 1000/T - 33.49\ (\pm 0.31) \quad (2)$$

Using the two equations, the averaged monthly drip water temperatures of 15.7 ± 0.5 °C, and a drip water $\delta^{18}O$ mean of $-6.90 \pm 0.03‰$ ($1\sigma_m$) in the Great Hall, the

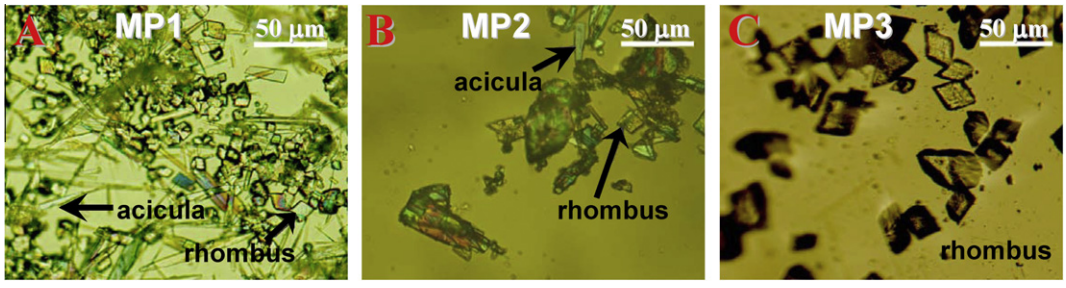

Fig. 8. Morphological compositions of modern carbonate, deposited on glass plates, (A) MP1, (B) MP2, and (C) MP3. MP1 and MP2 are mixtures of rhombus and acicula, while MP3 is pure calcite rhombus.

calculated aragonite $\delta^{18}O$ is from −6.8‰ to −6.2‰ (Eq. (1); Kim et al., 2007) or from −6.6‰ to −6.4‰ (Eq. (2); Patterson et al., 1993). The $\delta^{18}O$ values of active speleothems (−6.60 ± 0.18‰; Section 4.4.2) and very young top parts of stalagmites (−6.28‰ for FR0510-1 and −6.38‰ for FR5) agree with the calculated values. It demonstrates that the aragonite precipitates at oxygen isotopic equilibrium in Furong Cave.

Two morphologies formed on *in situ* glass plates (Fig. 8). A mixture of 10–50-μm acicula and rhombus is observable on glass plates MP1 and MP2. On plate MP3, only rhombohedral calcite with a $\delta^{18}O$ value of −6.85‰ precipitated. Using an oxygen isotope fractionations of 0.4–0.8‰ between equilibrium aragonite–water and calcite–water systems (e.g., Tarutani et al., 1969; Patterson et al., 1993; Kim et al., 2007), the derived possible aragonite $\delta^{18}O$ is from −6.45‰ to −6.05‰, which is consistent with the calculated range and the measured values of top subsamples of active speleothems. This agreement supports that Furong Cave stalagmite grew at an oxygen isotopic equilibrium condition.

4.7. Aragonite stalagmite $\delta^{18}O$

Oxygen data of waters and carbonates show that the modern aragonite stalagmites have deposited at oxygen isotopic equilibrium in Furong Cave (Section 4.6). To carefully assess the ability of these stalagmites to serve as paleoclimate archives, we need to consider the following three important factors in more detail.

4.7.1. Mineral transformation

The first is the aragonite-to-calcite transformation, which has been observed to occur as quickly as a couple hundred years, with 99% replacement at 1.2 thousand years ago, in Grotte de Clamouse, France (Frisia et al., 2002). The *in situ* EBSD techniques show that the mineral composition is 100% aragonite for depth 5.2 cm (1.4 ka) of FR0510-1 and for the depths of 11 cm (11.3 ka), 12 cm (12.1 ka), and 22 cm (16.1 ka) of FR5, and with only 0.013% intrusive calcite at the depth of 22 cm (Fig. 5). The absence of an aragonite-to-calcite transformation indicates that no post-depositional recrystallization took place on FR5 over the past 16 thousand years.

4.7.2. Hendy Test

The second factor is the well-known Hendy Test (Hendy, 1971) (Fig. 9). Despite $\delta^{13}C$ values vary from 0.7‰ to 1.3‰ for coeval subsamples on five selected layers of stalagmite FR5 (Fig. 9A), only a small $\delta^{18}O$ variation of ±0.11–0.19‰ for different fabrics on individual horizons (Fig. 9B) is observed. There is no relationship between $\delta^{18}O$ and $\delta^{13}C$ values (Fig. 9C). Combined with the water-active speleothem data (see Section 4.4.2), the evidences indicate that the stalagmite formed under oxygen isotopic equilibrium conditions.

4.7.3. Comparison of Chinese stalagmite $\delta^{18}O$ records

The third factor is the contemporaneity of stalagmite $\delta^{18}O$ records from different settings (e.g., Wang et al., 2001, 2008), which has been emphasized in review articles (e.g., Fairchild et al., 2006; Lachniet, 2009). The FR5 $\delta^{18}O$ values range from −3.8‰ to −8.5‰ between 16 and 6 kyr BP. The FR5 $\delta^{18}O$ record has a sharp decrease of 3.5‰ over the EAM Termination I and an ^{18}O enrichment of 2‰ at the Younger Dryas (YD) (Fig. 10). The amplitude and timing of the $\delta^{18}O$ changes in records of FR5, Hulu H82/YT (Wang et al., 2001), and Dongge D4 (Yuan et al., 2004; Dykoski et al., 2005) are not significantly different within dating errors. Synchroneity of these climate events between cave records indicate that the FR5 $\delta^{18}O$ record expresses regional-scale conditions.

Shifts of Chinese cave $\delta^{18}O$ data have been considered to be changes in the ratio of summer to winter precipitation (Wang et al., 2001) or simplified to reflect summer precipitation and relate to summer EAM variability (Yuan et al., 2004; Wang et al., 2008; Cheng et al., 2009). In addition to the cave hydrological condition (Fairchild et al., 2006;

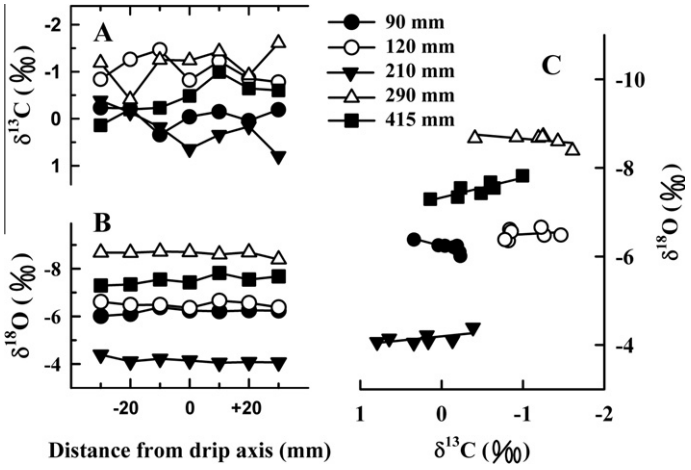

Fig. 9. Hendy Test on five laminae, at 90 mm (solid circles), 120 mm (hollow circles), 210 mm (solid triangles), 290 mm (hollow triangles), and 415 mm (solid squares) of the stalagmite FR5. (A) Coeval $\delta^{13}C$ data show remarkable differences of ±0.20–0.41‰. Small changes of ±0.11–0.19‰ observed for (B) coeval $\delta^{18}O$ data and (C) an absence of relationship between $\delta^{18}O$ and $\delta^{13}C$ indicate insignificant kinetic fractionation.

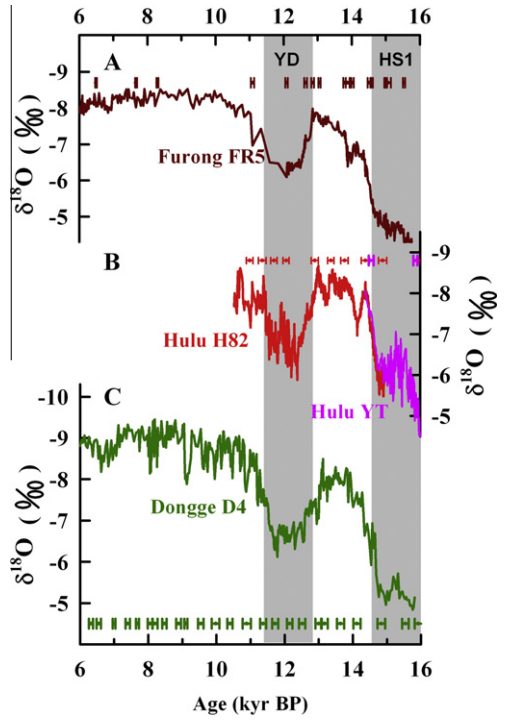

Fig. 10. Comparison of stalagmite $\delta^{18}O$ records of (A) Furong FR5, (B) Hulu H82/YT (Wang et al., 2001), and (C) Dongge D4 (Yuan et al., 2004; Dykoski et al., 2005) during 16–6 kyr BP. ^{230}Th ages and 2σ errors are color-coded by stalagmite. Hulu ^{230}Th dates are from Wang et al. (2004b). Shaded bands represent cold periods in Greenland, Heinrich stadial 1 (HS1, 17.5–14.5 kyr BP, Broecker and Barker, 2007) and YD. (For interpretation of the references to color in this figure legend, the reader is referred to the web version of this article.)

Lachniet, 2009), the speleothem $\delta^{18}O$ in the Chinese EAM region is attributed to changes of sea surface temperature and marine oxygen isotopic composition (Wang et al., 2008), shifts of moisture sources (Maher, 2008) and rainfall patterns (Cheng et al., 2009), and isotopic fractionation associated with atmospheric transport (Wei and Lin, 1994). This precipitation proxy has thus been adopted as a qualitative index of summer EAM intensity (after Wang et al., 2001). The consistency of three cave records from central (Furong), eastern (Hulu) and southern (Dongge) China supports the inferred EAM variability, with an orbitally-controlled long-term trend punctuated by millennial-scale events, such as Weak Monsoon Intervals (Cheng et al., 2009) and Chinese interstadials (Wang et al., 2001). These were driven primarily by high-latitudinal forcings in the Northern Hemisphere (e.g., Wang et al., 2001; Cheng et al., 2009). However, the decoupling of intensified summer EAM (Fig. 10) and decreasing temperatures in Greenland (Steffensen et al., 2008) during the Bølling–Allerød (BA) could have resulted from an interhemispheric bipolar see-saw mechanism. A strengthened winter Australian monsoon would enhance cross-equatorial moisture and heat transport from low latitudinal oceans to the northern hemisphere, which induced the strong summer EAM during the BA (An, 2000; Shen et al., 2010).

4.7.4. Discrepancy of a weak inferred summer EAM at 14.0 kyr BP between Chinese cave records

Although the general consistency of Chinese cave-inferred climate sequences between Chinese cave $\delta^{18}O$ (Fig. 10), there is one notable exception at 14.0 kyr BP. A 130-yr weak summer EAM in the Furong FR5 record is aligned with the 120-yr Older Dryas (OD) event in Greenland ice cores in timing and duration (Fig. 11). This event is also concurrently shown in Yamen Cave, Guizhou Province, China (Yang et al., 2010). However, this weak summer EAM lasted 230 yrs at 14.2 kyr BP in the Hulu H82 record, which is asynchronous with the event in Furong Cave, Yamen Cave, and Greenland NGRIP ice-core $\delta^{18}O$ records (Fig. 11). This +200-yr discrepancy indicates almost no perfect stalagmite age models due to variable deposition rates and limited absolute-dated layers, which should be considered for comparison of cave proxy records and also

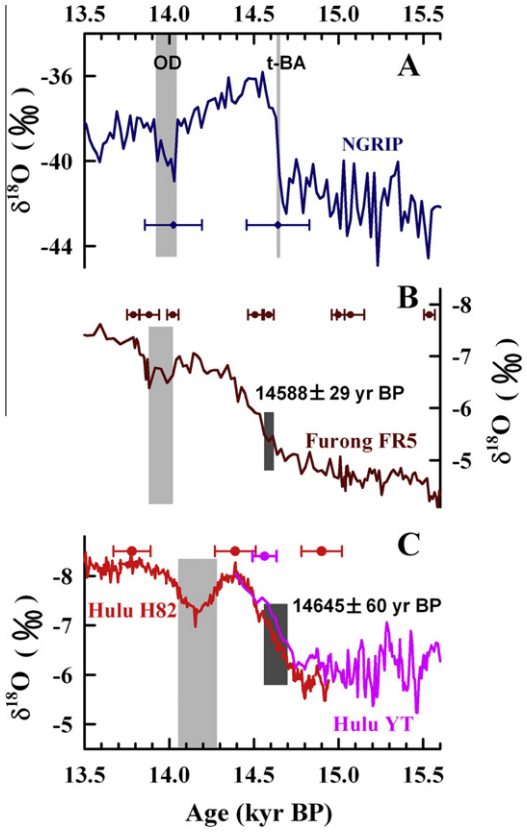

Fig. 11. Comparison of proxy records from Greenland and Chinese caves during 15.6–13.5 kyr BP. (A) Greenland NGRIP ice core $\delta^{18}O$ record [GICC05 timescale (NGRIP, 2006)]. The error bars indicate 2σ age uncertainties at the t-BA and the onset of OD. Shaded bands represent t-BA and OD. (B) Furong aragonite stalagmite FR5 $\delta^{18}O$. (C) $\delta^{18}O$ records of Hulu calcite stalagmites H82 and YT (Wang et al., 2001) with updated ^{230}Th dates (Wang et al., 2004b). ^{230}Th ages and 2σ errors are color-coded by stalagmite. Gray shaded bands denote the weak EAM in Furong and Hulu Caves. Dark shaded bands represent individual 2σ age uncertainties of the t-BA (see text). (For interpretation of the references to color in this figure legend, the reader is referred to the web version of this article.)

between different natural archives. Another possibility is the climatic responses could be spatially asynchronous in mainland China.

4.7.5. Advantages of high precision and resolution

The ppm uranium levels in Furong aragonite stalagmite allow for precise ^{230}Th dating, producing tight temporal constraints on the timing and duration of climatic events. The timing of the transition into the BA (t-BA) at Termination I is 14,645 ± 60 yr BP according to Hulu records (Fig. 11), a figure which was estimated using annual band counting and ^{230}Th dates on 1–1.5 g of powdered subsamples from 2-mm width horizons of stalagmite YT (Wang et al., 2001). The ^{230}Th age, 14,563 ± 71 yr BP, at a depth of 2.6 mm on stalagmite YT with a U content of 108 ppb (Wang et al., 2001), covers a wide time interval of 170 yrs, estimated with a growth rate of 0.012 mm/yr between depths of 1.6–3.4 mm (14,489–14,639 yr BP; Wang et al., 2001). In Furong Cave, t-BA can be determined directly at 14,588 ± 29 yr BP from 53 mg carbonate with high U content (5.2 ppm). The sample for this measurement was drilled from a narrow 1-mm horizon and corresponds to only 48 yrs of deposition.

5. CONCLUSIONS

Two-year observations of δ^{18}O and δ^{13}C-DIC dynamics in water samples in the Furong Cave are characterized by three features. (1) The infiltrating rainwater was homogenized with a residence time longer than 1 yr in the upper 300–500-m vadose zone. (2) Monthly variability of cave water δ^{18}O was repressed and drip water δ^{18}O represents the weighted average δ^{18}O values of regional precipitation. (3) With the evidence of 19-month cave air CO_2 records, the seasonal δ^{13}C-DIC variations of 5–7‰ in the pool water and of 2–3‰ in drip water could be attributed to seasonal soil CO_2 production and a kinetic degassing processes. Active speleothems show the aragonite deposition at oxygen isotopic equilibrium; while complicated carbon isotopic fractionation is observed. Our systematic hydrological and cave monitoring program first demonstrate the climatic applicability of aragonite stalagmite δ^{18}O. The coherent stalagmite oxygen isotope variations in Furong, Hulu and Dongge Caves at the t-BA and during the YD offer the direct robustness of paleoclimatic interpretation for Chinese cave δ^{18}O records in the EAM province. However, the 200-yr discrepancy of a weak summer EAM at 14.0 kyr BP between Hulu and other Chinese caves may result from different regional hydrological conditions or chronological uncertainty of stalagmite proxy time series with limited dating points and variable growth rates. Clearly, ppm-U-level aragonite stalagmites from Furong Cave can offer precise chronological control for inferred climatic/environmental events and further understanding the timing of dynamical forcings responsible for past climate variability.

ACKNOWLEDGMENTS

We thank the Management Department of Furong Cave for great help in the field since 2005. We thank Dr. I.J. Fairchild of the University of Birmingham, Dr. G.S. Burr of the University of Arizona, Dr. C.-H. Wang of the Academia Sinica, Dr. Y.-J. Wang of the Nanjing Normal University, and Dr. H.-S. Mii of the National Taiwan Normal University for constructive comments. This work was funded by the Open Foundation of the Karst Dynamics Laboratory, China (GKN0842008, KDL2008-08), the National Science Foundation of China (NSFC, 40802035), the Open Foundation of the State Key Laboratory of Loess and Quaternary Geology, Institute of Earth Environment, CAS, China (SKLLQG0907) and the Key Project of Special Research Foundation of Southwest University, China (XDJK2009B016) to L.T.Y., and (XDJK2009C106) to L.J.Y. Funding for this study was also provided by NSFC grants (40971122) to W.J.L., the Chongqing Science & Technology Commission (CSTC, 2009BA0002) to X.S.Y. and NSC grants (95-2752-M002-012-011-PAE, 97-2745-M-002-009, 98-2661-M-002-006, and 98-2116-M-002-012 to C.C.S.).

REFERENCES

Affek H. P., Bar-Matthews M., Ayalon A., Matthews A. and Eiler J. M. (2008) Glacial/interglacial temperature variations in Soreq cave speleothems as recorded by 'clumped isotope' thermometry. *Geochim. Cosmochim. Acta* **72**, 5351–5360.

An Z. (2000) The history and variability of the East Asian paleomonsoon climate. *Quatern. Sci. Rev.* **19**, 171–187.

Baker A., Ito E., Smart P. L. and McEwan R. F. (1997) Elevated and variable values of ^{13}C in speleothems in a British cave system. *Chem. Geol.* **136**, 263–270.

Baker A., Asrat A., Fairchild I. J., Leng M. J., Wynn P. M., Bryan C., Genty D. and Umer M. (2007) Analysis of the climate signal contained within δ^{18}O and growth rate parameters in two Ethiopian stalagmites. *Geochim. Cosmochim. Acta* **71**, 2975–2988.

Bar-Matthews M., Ayalon A., Matthews A., Sass E. and Halicz L. (1996) Carbon and oxygen isotope study of the active water–carbonate system in a karstic Mediterranean cave: implications for paleoclimate research in semiarid regions. *Geochim. Cosmochim. Acta* **60**, 337–347.

Bar-Matthews M., Ayalon A. and Kaufman A. (1997) Late Quaternary paleoclimate in the Eastern Mediterranean region from stable isotope analysis of speleothems at Soreq Cave, Israel. *Quatern. Res.* **47**, 155–168.

Bar-Matthews M., Ayalon A., Gilmour M., Matthews A. and Hawkesworth C. J. (2003) Sea-land oxygen isotopic relationships from planktonic foraminifera and speleothems in the Eastern Mediterranean region and their implication for paleorainfall during interglacial intervals. *Geochim. Cosmochim. Acta* **67**, 3181–3199.

Böhm F., Joachimski M. M., Dullo W. C., Eisenhauer A., Lehnert H., Reitner J. and Wörheide G. (2000) Oxygen isotope fractionation in marine aragonite of coralline sponges. *Geochim. Cosmochim. Acta* **64**, 1695–1703.

Breecker D. O., Sharp Z. D. and McFadden L. D. (2009) Seasonal bias in the formation and stable isotopic composition of pedogenic carbonate in modern soils from central New Mexico, USA. *Geol. Soc. Am. Bull.* **121**, 630–640.

Broecker W. and Barker S. (2007) A 190‰ drop in atmosphere's Δ^{14}C during the "Mystery Interval" (17.5 to 14.5 kyr). *Earth Planet. Sci. Lett.* **256**, 90–99.

Buggisch W., Keller M. and Lehnert O. (2003) Carbon isotope record of Late Cambrian to Early Ordovician carbonates of the Argentine Precordillera. *Palaeogeogr. Palaeoclimatol. Palaeoecol.* **195**, 357–373.

Cheng H., Edwards R. L., Hoff J., Gallup C. D., Richards D. A. and Asmersom Y. (2000) The half-lives of uranium-234 and thorium-230. *Chem. Geol.* **169**, 17–33.

Cheng H., Edwards R. L., Broecker W. S., Denton G. H., Kong X., Wang Y., Zhang R. and Wang X. (2009) Ice age terminations. *Science* **326**, 248–252.

Cosford J., Qing H., Eglington B., Mattey D., Yuan D., Zhang M. and Cheng H. (2008) East Asian monsoon variability since the Mid-Holocene recorded in a high-resolution, absolute-dated aragonite speleothem from eastern China. *Earth Planet. Sci. Lett.* **295**, 219–230.

Cruz F. W., Vuille M., Burns S. J., Wang X., Cheng H., Werner M., Edwards R. L., Karmann I., Auler A. S. and Nguyen H. (2009) Orbitally driven east–west antiphasing of South American precipitation. *Nat. Geosci.* **2**, 210–214.

Dan S.-M., Dan B., Xu H.-X., Chen G.-Y. and An H.-F. (2008) Calculation and discussion on correcting model of the potential temperature above complex terrain based on NOAA/AVHRR and DEM. *Int. Arch. Photogramm. Remote Sens. Spatial Inf. Sci.* **37**(Pt. B8), 577–582.

Dayem K. E., Molnar P., Battisti D. S. and Roe G. H. (2010) Lessons learned from oxygen isotopes in modern precipitation applied to interpretation of speleothem records of paleoclimate from eastern Asia. *Earth Planet. Sci. Lett.* **295**, 219–230.

Denniston R. F., DuPree M., Dorale J. A., Asmeron Y., Polyak V. J. and Carpenter S. J. (2007) Episodes of late Holocene aridity recorded by stalagmites from Devil's Icebox Cave, central Missouri, USA. *Quatern. Res.* **68**, 45–52.

Dorale J. A., Edwards R. L., González L. and Ito E. (1998) Climate and vegetation history of the midcontinent from 75 to 25 ka: a speleothem record from Crevice Cave, Missouri, USA. *Science* **282**, 1871–1874.

Dulinski M. and Rozanski K. (1990) Formation of $^{13}C/^{12}C$ isotope ratios in speleothems: a semi-dynamic model. *Radiocarbon* **32**, 7–16.

Dykoski C. A., Edwards R. L., Cheng H., Yuan D., Cai Y., Zhang M., Lin Y., Qing J., An Z. and Revenaugh J. (2005) A high-resolution, absolute-dated Holocene and deglacial Asian monsoon record from Dongge Cave, China. *Earth Planet. Sci. Lett.* **233**, 71–86.

Fairchild I. J., Smith C. L., Baker A., Fuller L., Spötl C., Mattey D. and McDermott F.EIMF (2006) Modification and preservation of environmental signals in speleothems. *Earth-Sci. Rev.* **75**, 105–153.

Finch A. A., Shaw P. A., Weedon G. P. and Holmgren K. (2001) Trace element variation in speleothem aragonite: potential for palaeoenvironmental reconstruction. *Earth Planet. Sci. Lett.* **186**, 255–267.

Finch A. A., Shaw P. A., Holmgren K. and Lee-Thorp J. (2003) Corroborated rainfall records from aragonitic stalagmites. *Earth Planet. Sci. Lett.* **215**, 265–273.

Fleitmann D., Burns S. J., Manginic A., Mudelseed M., Kramersa J., Villaa I., Neff U., Al-Subbarye A. A., Buettner A., Hipplera D. and Matter A. (2007) Holocene ITCZ and Indian monsoon dynamics recorded in stalagmites from Oman and Yemen (Socotra). *Quatern. Sci. Rev.* **26**, 170–188.

Frappier A. B., Sahagian D., Carpenter S. J., González L. A. and Frappier B. R. (2007) Stalagmite stable isotope record of recent tropical cyclone events. *Geology* **35**, 111–114.

Frisia S., Borsato A., Fairchild I. J. and McDermott F. (2000) Calcite fabrics, growth mechanisms, and environments of formation in speleothems from the Italian Alps and southwestern Ireland. *J. Sed. Res.* **70**, 1183–1196.

Frisia S., Borsato A., Fairchild I. J., McDermott F. and Selmo E. M. (2002) Aragonite–calcite relationships in speleothems (Grotte de Clamouse, France): environment, fabrics, and carbonate geochemistry. *J. Sed. Res.* **72**, 687–699.

Frisia S., Fairchild I. J., Fohlmeister J., Miorandi R., Spötl C. and Borsato A. (2011) Carbon mass-balance modelling and carbon isotope exchange processes in dynamic caves. *Geochim. Cosmochim. Acta* **75**, 380–400.

Frohlich C., Hornbach M. J., Taylor F. W., Shen C.-C., Moala A., Morton A. E. and Kruger J. (2009) Huge erratic boulders in Tonga deposited by a prehistoric tsunami. *Geology* **37**, 131–134.

Genty D., Baker A., Massault M., Proctor C., Gilmour M., Pons-Branchu E. and Hamelin B. (2001) Dead carbon in stalagmites: carbonate bedrock paleodissolution vs. ageing of soil organic matter. Implications for ^{13}C variations in speleothems. *Geochim. Cosmochim. Acta* **65**, 3443–3457.

Grossman E. L. and Ku T.-L. (1986) Oxygen and carbon isotope fractionation in biogenic aragonite: temperature effects. *Chem. Geol.* **59**, 59–74.

Hellstrom J., Mcculloch M. and Stone J. (1998) A detailed 31,000-year record of climate and vegetation change, from the isotope geochemistry of two New Zealand speleothems. *Quatern. Res.* **50**, 167–178.

Hendy C. H. (1971) The isotopic geochemistry of speleothem: part 1. the calculation of the effects of different modes of formation on the isotopic composition of speleothems and their applicability as palaeoclimatic indicators. *Geochim. Cosmochim. Acta* **35**, 801–824.

Hill C. and Forti P. (1997) *Cave Minerals of the World*, second ed. National Speleological Society, Huntsville, Alabama.

Jaffey A. H., Flynn K. F., Glendenin L. E., Bentley W. C. and Essling A. M. (1971) Precision measurement of half-lives and specific activities of ^{235}U and ^{238}U. *Phys. Rev.* **4**, 1889–1906.

Johnson K. R., Hu C., Belshaw N. S. and Henderson G. M. (2006) Seasonal trace element and stable-isotope variations in a Chinese speleothem: the potential for high-resolution paleomonsoon reconstruction. *Earth Planet. Sci. Lett.* **244**, 394–407.

Kim S. T., O'Neil J. R., Hillaire-Marcel C. and Mucci A. (2007) Oxygen isotope fractionation between synthetic aragonite and water: influence of temperature and Mg^{2+} concentration. *Geochim. Cosmochim. Acta* **71**, 4704–4715.

Lachniet M. S. (2009) Climatic and environmental controls on speleothem oxygen-isotope values. *Quatern. Sci. Rev.* **28**, 412–432.

Lambert W. J. and Aharon P. (2011) Controls on dissolved inorganic carbon and $\delta^{13}C$ in cave waters from DeSoto Caverns: implications for speleothem $\delta^{13}C$ assessments. *Geochim. Cosmochim. Acta* **75**, 753–768.

Li H.-C., Lee Z.-H., Wan N.-J., Shen C.-C., Li T.-Y., Yuan D. and Chen Y.-H. (2011) The $\delta^{18}O$ and $\delta^{13}C$ records in an aragonite stalagmite from Furong Cave, Chongqing, China: a-2000-year record of monsoonal climate. *J. Asian Earth Sci.* **40**, 1121–1130.

Li T.-Y., Yuan D., Li H.-C., Yang Y., Wang J., Wang X., Li J., Qin J., Zhang M. and Lin Y. (2007) High-resolution climate variability of southwest China during 57–70 ka reflected in a stalagmite $\delta^{18}O$ record from Xinya Cave. *Sci. China D* **50**, 1202–1208.

Li T.-Y., Li H.-C., Shen C.-C., Yang C., Li J., Yi C. and Yuan D. (2010) Primary study on the δD and $\delta^{18}O$ characteristics of meteoric precipitation during 2006–2008 in Chongqing, China. *Adv. Water. Sci.* **21**, 757–764 (in Chinese).

Liu K., Ding X., Fu D., Pan Y., Wu X., Guo Z. and Zhou L. (2007) A new compact AMS system at Peking University. *Nucl. Instrum. Methods Phys. Res. B* **259**, 23–26.

Maher B. A. (2008) Holocene variability of the East Asian summer monsoon from Chinese cave records: a re-assessment. *Holocene* **18**, 861–866.

Mattey D., Lowry D., Duffet J., Fisher R., Hodge E. and Frisia S. (2008) A 53 year seasonally resolved oxygen and carbon isotope record from a modern Gibraltar speleothem: reconstructed drip water and relationship to local precipitation. *Earth Planet. Sci. Lett.* **269**, 80–95.

McConnaughey T. (1989) C-13 and O-18 isotopic disequilibrium in biological carbonates: 1. patterns. *Geochim. Cosmochim. Acta* **53**, 151–162.

McCrea J. M. (1950) On the isotopic chemistry of carbonates and a paleotemperature scale. *J. Chem. Phys.* **18**, 849–857.

McDermott F., Frisia S., Huang Y. M., Longinelli A., Spiro B., Heaton T. H. E., Hawkesworth C. J., Borsato A., Keppens E., Fairchild I. J., van der Borg K., Verheyden S. and Selmo E. (1999) Holocene climate variability in Europe: evidence from $\delta^{18}O$, textural and extension-rate variations in three speleothems. *Quatern. Sci. Rev.* **18**, 1021–1038.

McDermott F. (2004) Palaeo-climate reconstruction from stable isotope variations in speleothems: a review. *Quatern. Sci. Rev.* **23**, 901–918.

McMillan E. A., Fairchild I. J., Frisia S., Borsato A. and McDermott F. (2005) Annual trace element cycles in calcite–aragonite speleothems: evidence of drought in the western Mediterranean 1200–1100 yr BP. *J. Quatern. Sci.* **20**, 423–433.

Miorandi R., Borsato A., Frisia S., Fairchild I. J. and Richter D. K. (2010) Epikarst hydrology and implications for stalagmite capture of climate changes at Grotta di Ernesto (NE Italy): results from long-term monitoring. *Hydrol. Process.* **24**, 3101–3114.

Morse J. W., Wang Q. and Tsio M. Y. (1997) Influences of temperature and Mg:Ca ratio on $CaCO_3$ precipitates from seawater. *Geology* **25**, 85–87.

Neff U., Burns S. J., Mangini A., Mudelsee M., Fleitmann D. and Matter A. (2001) Strong coherence between solar variability and the monsoon in Oman between 9 and 6 kyr ago. *Nature* **411**, 290–293.

Neuser R. D. and Richter D. K. (2007) Non-marine radiaxial fibrous calcites—examples of speleothems proved by electron backscatter diffraction. *Sed. Geol.* **194**, 149–154.

NGRIP Dating Group (2006) Greenland Ice Core Chronology 2005 (GICC05), IGBP PAGES/World Data Center for Paleoclimatology, Data Contribution Series #2006-118. NOAA/NCDC Paleoclimatology Program, Boulder CO, USA.

Ortega R., Maire R., Devès G. and Quinif Y. (2005) High-resolution mapping of uranium and other trace elements in recrystallized aragonite–calcite speleothems from caves in the Pyrenees (France): implication for U-series dating. *Earth Planet. Sci. Lett.* **237**, 911–923.

Patterson W. P., Smith G. R. and Lohmann K. C. (1993) Continental paleothermometry and seasonality using the isotopic composition of aragonite otoliths of freshwater fishes. In *Climate Change in Continental Isotopic Records*, vol. 78 (eds. P. K. Swart, C. K. Lohmann, J. Mckenzie and S. Savin). *Geophys. Monogr. Ser.*, pp. 191–202.

Perrette Y., Delannoy J. J., Bolvin H., Cordonnier M., Destombes J. L., Zhilinskaya E. A. and Aboukais A. (2000) Comparative study of a stalagmite sample by stratigraphy, laser induced fluorescence spectroscopy, EPR spectrometry and reflectance imaging. *Chem. Geol.* **16**, 221–243.

Railsback L. B., Brook G. A., Chen J., Kalin R. and Fleisher C. J. (1994) Environmental controls on the petrology of a last Holocene speleothem from Botswana with annual layers aragonite and calcite. *J. Sed. Res. A: Sed. Petrol. Proc.* **64**, 147–155.

Reimer P. J., Baillie M. G. L., Bard E., Bayliss A., Beck J. W., Blackwell P. G., Bronk Ramsay C., Buck C. E., Burr G. S., Edwards R. L., Friedrich M., Grootes P. M., Guilderson T. P., Hajdas B., Heaton T. J., Hogg A. G., Hughen K. A., Kaiser K. F., Kromer B., McCormac F. G., Manning S. W., Reimer R. W., Richards D. A., Southon J. R., Talamo S., Turney C. S. M., van der Plicht J. and Weyhenmeyer C. E. (2009) IntCal09 and Marine09 radiocarbon age calibration curves, 0–50,000 years cal BP. *Radiocarbon* **51**, 1111–1150.

Richards D. A. and Dorale J. A. (2003) Uranium-series chronology and environmental applications of speleothems. In *Uranium-Series Geochemistry* (eds. B. Bourdon, G. M. Henderson, C. C. Lundstrom and S. P. Turner). Mineralogical Society of America, Washington, DC, pp. 407–460.

Shen C.-C., Edwards R. L., Cheng H., Dorale J. A., Thomas R. B., Moran S. B., Weinstein S. E. and Edmonds H. N. (2002) Uranium and thorium isotopic and concentration measurements by magnetic sector inductively coupled plasma mass spectrometry. *Chem. Geol.* **185**, 165–178.

Shen C.-C., Cheng H., Edwards R. L., Moran S. B., Edmonds H. N., Hoff J. A. and Thomas R. B. (2003) Measurement of attogram quantities of ^{231}Pa in dissolved and particulate fractions of seawater by isotope dilution thermal ionization mass spectroscopy. *Anal. Chem.* **75**, 1075–1079.

Shen C.-C., Li K.-S., Sieh K., Natawidjaja D., Cheng H., Wang X., Edwards R. L., Lam D. D., Hsieh Y.-T., Fan T.-Y., Meltzner A. J., Taylor F. W., Quinn T. M., Chiang H.-W. and Kilbourne K. H. (2008) Variation of initial $^{230}Th/^{232}Th$ and limits of high precision U–Th dating of shallow-water corals. *Geochim. Cosmochim. Acta* **72**, 4201–4223.

Shen C.-C., Kano A., Hori M., Lin K., Chiu T.-C. and Burr G. S. (2010) East Asian monsoon evolution and reconciliation of climate records from Japan and Greenland during the last deglaciation. *Quatern. Sci. Rev.* **29**, 3327–3335.

Spötl C., Fairchild I. J. and Tooth A. F. (2005) Cave air control on dripwater geochemistry, Obir Caves (Austria): implications for speleothem deposition in dynamically ventilated caves. *Geochim. Cosmochim. Acta* **69**, 2451–2468.

Steffensen J. P., Andersen K. K., Bigler M., Clausen H. B., Dahl-Jensen D., Fischer H., Goto-Azuma K., Hansson M., Johnsen S. J., Jouzel J., Masson-Delmotte V., Popp T., Rasmussen S. O., Röthlisberger R., Ruth U., Stauffer B., Siggaard-Andersen M.-L., Sveinbjörnsdóttir Á. E., Svensson A. and White J. W. C. (2008) High-resolution Greenland ice core data show abrupt climate change happens in few years. *Science* **321**, 680–684.

Tan M., Hou J. and Cheng H. (2002) Methodology of quantitatively reconstructing paleoclimate from annually laminated stalagmites. *Quatern. Sci.* **22**, 209–219.

Tan L., Cai Y., An Z., Edwards R. L., Cheng H., Shen C.-C., Zhang H. (2010) Centennial- to decadal-scale monsoon precipitation variability in the semi-humid region, northern China during the last 1860 years: records from stalagmites in Huangye Cave. *Holocene*. doi:10.1177/0959683610378880.

Tarutani T., Clayton R. N. and Mayeda T. K. (1969) The effect of polymorphism and magnesium substitution on oxygen isotope fractionation between calcium carbonate and water. *Geochim. Cosmochim. Acta* **33**, 987–996.

Thorrold S. R., Campana S. E., Jones C. M. and Swart P. K. (1997) Factors determining $\delta^{13}C$ and $\delta^{18}O$ fractionation in aragonitic otoliths of marine fish. *Geochim. Cosmochim. Acta* **61**, 2909–2919.

Treble P. C., Chappell J., Gagan M. K., McKeegan K. D. and Harrison T. M. (2005) In situ measurement of seasonal delta O-18 variations and analysis of isotopic trends in a modem speleothem from southwest Australia. *Earth Planet. Sci. Lett.* **233**, 17–32.

Veizer J., Ala D., Azmy K., Bruckschen P., Buhl D., Bruhn F., Carden G. A. F., Diener A., Ebneth S., Godderis Y., Jesper T., Korte C., Pawellek F., Podlaha O. G. and Strauss H. (1999)

$^{87}Sr/^{86}Sr$, $\delta^{13}C$ and $\delta^{18}O$ evolution of phanerozoic seawater. *Chem. Geol.* **161**, 59–88.

Wang X., Auler A. S., Edwards R. L., Cheng H., Cristalli P. S., Smart P. L., Richards D. A. and Shen C.-C. (2004a) Wet periods in northeastern Brazil over the past 210 kyr linked to distant climate anomalies. *Nature* **432**, 740–743.

Wang X., Auler A. S., Edwards R. L., Cheng H., Ito E., Wang Y., Kong X. and Solheid M. (2007) Millennial-scale precipitation changes in southern Brazil over the past 90,000 years. *Geophys. Res. Lett.* **34**, L23701. doi:10.1029/2007GL031149.

Wang Y., Cheng H., Edwards R. L., An Z., Wu J., Shen C.-C. and Dorale J. A. (2001) A high-resolution absolute-dated late Pleistocene monsoon record from Hulu Cave, China. *Science* **294**, 2345–2348.

Wang Y., Cheng H., Edwards R. L., An Z., Wu J., Shen C.-C., Dorale J. A. (2004b) Hulu Cave Stalagmite Oxygen Isotope Data, IGBP, PAGES/World Data Center for Paleoclimatology, Data Contribution Series #2004-023. NOAA/NGDC Paleoclimatology Program, Boulder, Colorado, USA.

Wang Y., Cheng H., Edwards R. L., He Y., Kong X., Zn Z., Wu J., Kelly M. J., Dykoski C. A. and Li X. (2005) The Holocene Asian monsoon: links to solar changes and North Atlantic climate. *Science* **308**, 854–857.

Wang Y., Cheng H., Edwards R. L., Kong X., Shao X., Chen S., Wu J., Jiang X., Wang X. and An Z. (2008) Millennial- and orbital-scale changes in the east Asia monsoon over the past 224000 years. *Nature* **451**, 1090–1093.

Wei K. and Lin R. (1994) The influence of the monsoon climate on the isotopic composition of precipitation in China. *Geochimica* **23**, 33–41 (in Chinese).

Winograd I. J., Coplen T. B., Landwehr J. M., Riggs A. C., Ludwig K. R., Szabo B. J., Kolesar P. T. and Revesz K. M. (1992) Continuous 500,000-year climate record from vein calcite in Devils Hole, Nevada. *Science* **258**, 255–260.

Yang Y., Yuan D. X., Cheng H., Zhang M. L., Qin J. M., Lin Y. S., Zhu X. Y. and Edwards R. L. (2010) Precise dating of abrupt shifts in the Asian monsoon during the last deglaciation based on stalagmite data from Yamen Cave, Guizhou Province, China. *Sci. China D* **53**, 633–641.

Yuan D., Cheng H., Edwards R. L., Dykoski C. A., Kelly M. J., Zhang M., Qing J., Lin Y., Wang Y., Wu J., Dorale J. A., An Z. and Cai Y. (2004) Timing, duration, and transitions of the last interglacial Asian monsoon. *Science* **203**, 575–578.

Zheng Y. (1999) Oxygen isotope fractionation in carbonate and sulfate minerals. *Geochem. J.* **33**, 109–126.

Zhou G. and Zheng Y. (2003) An experimental study of oxygen isotope fractionation between inorganically precipitated aragonite and water at low temperatures. *Geochim. Cosmochim. Acta* **67**, 387–399.

Zhou H., Feng Y., Zhao J., Shen C.-C., You C.-F. and Lin Y. (2009) Deglacial variations of Sr and $^{87}Sr/^{86}Sr$ ratio recorded by a stalagmite from Central China and their association with past climate and environment. *Chem. Geol.* **268**, 233–247.

Associate editor: Miryam Bar-Matthews